SUPPLEMENTARY METHODS

Scaling of sensorimotor delays in terrestrial mammals
Heather L. More and J. Maxwell Donelan
Proceedings of the Royal Society B. DOI 10.1098/rspb.2018.0613

Component delay systematic reviews

In total, we used data from 73 independent studies and 12 species (tables S1—S6). Specifically, we considered measurements made *in vivo* near body temperature, on live adult quadrupedal mammals that were as close to wild type as possible. We accepted data that was measured or reported at close to normal core body temperature (between 35°C and 40°C); we included one measurement made below body temperature [1]. We also included thirteen studies that did not report the temperature at which their measurements were made, where we had reason to believe that their measurements were close to body temperature (e.g. tissue was covered in warmed mineral oil) and/or where their reported delays were no slower than those measured at body temperature in other studies on the same species.

We focused on measurements from the medial gastrocnemius but, due to scarcity of data, we included some measurements from additional lower limb muscles. For sensing delay, we included one measurement from the quadriceps [2] and one measurement pooling data from all ankle extensors [3]. For neuromuscular junction delay, we included one study reporting data from the peroneus tertius [4] and one study reporting data from the digital flexors [5]; these hindlimb muscles are innervated by branches of the sciatic nerve. For electromechanical delay and force generation delay, we included one study reporting values from the lateral gastrocnemius because the researchers stated that the delays in the medial and lateral gastrocnemius were not significantly different [6]. We also included one *in vitro* study of force generation delay in the extensor digitorum longus [7].

For studies that did not report the masses of their animals, we estimated the mass from a different publication on the same species, written by at least one co-author of the study in question, or from species growth charts for the appropriate strain and age; where this was not possible, we omitted the study from our calculation of average body mass. If there were insufficient studies to calculate average body mass for a given component delay within a species, we used the average species mass reported in [8].

Sensing delay

We searched for measurements of the time between the onset of stretch in the medial gastrocnemius and the onset of action potential generation in the associated Ia afferent fibers. We defined the onset of stretch as the time at which muscle length first deflected from its resting length, but did not impose restrictions on the method of muscle stretch.

Nerve conduction delay

We began by combining data from our previous experiments and systematic review to give nerve fiber conduction velocity values from eleven species [8, 9]. Previously, we found no evidence for consistent differences between conduction velocities in sensory and motor nerve fibers [8], so we simplified our analysis by assuming equal sensory and motor nerve fiber conduction velocities. For each species, we converted average hindlimb nerve fiber

conduction velocity to nerve conduction delay using leg length predicted from the species' average mass. To predict leg length, we derived a relationship between hindlimb length (in metres) and animal mass (M; in kilograms) by first predicting lengths of the femur, tibia, and metatarsals at 12 logarithmically-spaced masses spanning the range of animal masses used to establish these relationships [10], adding the lengths of these three bones at each mass to give total hindlimb length, logarithmically transforming the masses and corresponding leg lengths, then performing a least-squares linear regression to determine the exponent and coefficient of the power law:

$$\text{average hindlimb length} = 0.165M^{0.333}$$

During a stretch reflex, impulses are conducted along sensory and motor nerve fibers from the muscle to the spinal cord and back to the muscle – twice the distance between the muscle and the spinal cord. We approximated this as twice the leg length, reasoning that the neglected distance from the proximal femur to the spinal cord is comparable to the included distance from the ground to the distal leg muscles. Therefore, the nerve conduction delay (in milliseconds) in a stretch reflex is given by twice the leg length (in metres) divided by the nerve fiber conduction velocity (in metres per second) and multiplied by 1,000 (to convert from seconds to milliseconds):

$$\text{nerve conduction delay} = \frac{2(0.165)(1{,}000)}{\text{nerve fiber conduction velocity}} M^{0.333}$$

Synaptic delay

We searched for measurements of the time required to transfer an impulse across monosynaptic connections between sensory neurons and motor neurons in the lumbosacral spinal cord [11, 12].We included studies that stimulated Ia sensory nerve fibers either electrically or by muscle stretch, and that investigated nerve fibers innervating the medial gastrocnemius or other lower limb pathways; we included studies that stimulated and recorded from slightly different sites. We included studies that measured delay either to the initial change in conductance of the postsynaptic cell, or to the onset of the action potential in the postsynaptic cell – we anticipate that this accounts for the 0.2 ms difference between synaptic delay and neuromuscular junction delay, because all the neuromuscular junction delay studies that we included measured time to the onset of the action potential.

Neuromuscular junction delay

We searched for measurements of the time between the onset of an action potential in the nerve, measured close to the muscle, and the onset of electrical activity in the muscle.

Electromechanical delay

We searched for measurements from single-twitch non-potentiated responses made in intact medial gastrocnemius muscles at their resting length, and combined these with results from our previous experiments [9]. Where separate values for different types of motor units were given, we used values from fast or fast fatiguable fibers, because fast fibers have shorter electromechanical and force generation delays than slow fibers [6].

Specifically, we searched for measurements of the time between the onset of electrical activity in the muscle and the onset of force production. We considered measurements made

by stimulating either a single nerve fiber or the whole nerve while recording muscle activity and force, as well as measurements made by directly stimulating the muscle and recording muscle force. Both whole-nerve stimulation and direct muscle stimulation activate multiple motor units in the muscle, but because electromechanical delay is calculated based on the difference in signal onset times, the measured delay is likely due to the fastest motor units.

We included data for goat electromechanical delay, measured by Lee et al. during the same experiments from which we obtained goat force generation delay [13]. The first author kindly provided us these data, which were not published in the original study.

Force generation delay

As for electromechanical delay, we searched for measurements from single-twitch non-potentiated responses made in intact medial gastrocnemius muscles at their resting length, and combined these with results from our previous experiments [9]. Where separate values for different types of motor units were given, we used values from fast or fast fatiguable fibers, because fast fibers have shorter electromechanical and force generation delays than slow fibers [6].

Specifically, we searched for measurements of the time between the onset of muscle force production and peak force. To reduce variability in force onset time and the onset of peak force production, we focussed on measurements made by stimulating a single nerve fiber or by stimulating multiple fast motor units at the same time. If motor units were stimulated asynchronously, or if slow and fast motor units were stimulated at the same time, force generation delay would appear to be excessively long because the onset of force production would be driven by the faster muscle fibers whereas the time to peak force would be driven by the slower muscle fibers. Either or both of these scenarios could occur during whole-nerve stimulation [4], so we generally did not consider measurements made in this way. We included one study, however, which statistically reconstructed the fast motor unit force profile after stimulation of the entire nerve [13]. We also included two studies which simultaneously activated fast motor units by directly stimulating the surface of the medial gastrocnemius [7, 9], which contains mostly fast fibers [14-16].

Scaling of component delays

We fit log-transformed data because size-dependent biological variation tends to be multiplicative, rather than additive [17, 18]. We tested this assumption by examining the log-space residuals and found no systematic effect of size on residual magnitude [19].

Phylogenetically independent contrasts

For nerve conduction delay, electromechanical delay, and force generation delay, we conducted phylogenetically independent contrasts analyses to test for the influence of evolutionary history on our data [20]. For each of these three delays, we entered logarithmically transformed species averages into Mesquite 3.03 [21]. We constructed a phylogenetic tree for the species using recent estimates of mammalian divergence patterns ([22-24]; figure S1) and set all branch lengths equal to one, because rates of phenotypic change are not necessarily correlated with divergence times and because equal branch lengths show the lowest rate of Type I errors [25, 26].

For each of the three component delays, the PDAP:PDTREE module in Mesquite [27] determined whether there was a significant correlation between the contrasts and their standard deviations; all relationships were insignificant (p-values ranged from 0.5 to 0.8). We inspected the contrasts for deviations from a normal distribution and for outliers; we found none. We therefore inferred that our data fulfilled the assumptions of independent contrasts analysis.

Finally, we investigated the phylogenetically-corrected relationships between our logarithmically transformed species averages. Least squares regression of the contrasts of the transformed delays on the contrasts of the transformed masses gave slopes similar to those of our original uncorrected regressions (tables 1 and S7); reduced major axis regression and major axis regression gave only slightly different results than linear regression. All phylogenetically-corrected relationships were significant ($p<0.05$; table S7). These results indicate our data are not greatly affected by evolutionary history, so we continued without adjusting for phylogenetic relatedness.

Scaling of total delay

We estimated the scaling relationship for total delay by fitting a power law to the sums of predicted component delays at a range of masses. This was necessary because we did not have data for all component delays in each individual species, and because the sum of power laws is not necessarily also a power law. We used the power law relationships identified for each component delay to predict component delays at 12 different masses that logarithmically spanned the range of animal masses we studied, from 0.0022 to 3,860 kilograms. For each mass, we added the predicted component delays to find total delay. Least-squares linear regression of the logarithmically transformed masses and corresponding total delays determined the exponent and coefficient of the power law approximating the relationship between animal mass and total delay.

Scaling of relative delay

We calculated relative delay at two speeds: the trot-gallop transition, because it is a physiologically similar speed for animals of different sizes [28], and maximum sprint speed, because it has the shortest stance phase and is important for survival activities such as catching prey and escaping predators. At each speed, we expressed total delay relative to stride duration – the time elapsed between consecutive contacts of a limb with the ground – and relative to stance duration – the time elapsed between the contact of a limb with the ground and when it leaves the ground. At both speeds, we first determined the power law relationship between mass and stride duration, then between mass and stance duration. We divided the power law relationship for total delay by these to determine relative delay.

Trot-gallop transition

We first found a relationship between mass M (in kilograms) and stride period $T_{\text{trot-gallop}}$ (in seconds) by inverting the known relationship between mass and stride frequency $f_{\text{trot-gallop}}$ (in minutes^{-1}) at the trot-gallop transition speed, and multiplying by 60,000 (to convert from minutes to milliseconds) [28]:

$$f_{\text{trot-gallop}} = 269M^{-0.14}$$

$$T_{\text{trot-gallop}} = \frac{60{,}000}{269}M^{0.14}$$

$$= 223M^{0.14}$$

Regardless of body mass, the stance phase of most quadrupeds running at their trot-gallop transition comprises a similar fraction of their stride period. This fraction is referred to as duty factor, and has been measured as approximately 0.42 (s.d.=0.03) for the hindlimb at the trot-gallop transition [29]. We multiplied stride period by duty factor to find the relationship between mass and stance duration at the trot-gallop transition:

$$\text{stance duration}_{\text{trot-gallop}} = (0.42)(223M^{0.14})$$

$$= 93.68M^{0.14}$$

For a typical 1 kg animal, this relationship indicates that the duration of stance phase will be approximately 94 milliseconds at the trot-gallop transition

Maximum sprint speed

We first found a relationship between mass M (in kilograms) and stride period T_{max} (in milliseconds). Because stride period has not been directly measured in animals with a range of sizes at maximum sprint speed, we estimated this relationship by inverting the known relationship between mass and stride frequency $f_{\text{sustained}}$ (in seconds^{-1}) at maximum sustained running speed [30], dividing by 1.1 to correct for the 10% increase in stride frequency (and corresponding decrease in stride period) as speed doubles from sustained speed to maximum speed [30, 31], and multiplying by 1,000 (to convert from seconds to milliseconds):

$$f_{\text{sustained}} = 4.7\text{M}^{-0.16}$$

$$T_{\text{max}} = \frac{1{,}000}{(4.7)(1.1)}M^{0.16}$$

$$= 193M^{0.16}$$

The duty factor of animals running at their maximum speed is not consistent across animal size [32]. However, because duty factor is related to the dimensionless speed given by the Froude number [32], we used the Froude number at maximum sprint speed to calculate duty factor. Froude number Fr is given by:

$$Fr = \frac{v}{\sqrt{gh}}$$

where v is velocity (in metres per second), g is acceleration due to gravity (here equal to 9.81 m/s^2), and h is hip height (in metres) [32]. The relationship between duty factor df and Froude number Fr is slightly different for cursorial and non-cursorial animals, so we approximated the relationship for our range of species by averaging the coefficients and exponents of the two respective power laws [32]; we also adjusted for the different definition of Froude number by doubling the exponent:

$$df = \frac{0.53 + 0.56}{2} Fr^{2\left(\frac{-0.28-0.18}{2}\right)}$$
$$= 0.545 Fr^{-0.46}$$

We substituted the scaling relationships for velocity [33] and hip height [34] into the Froude number relationship to determine how Froude number $Fr_{\max}$ at maximum sprint speed scales with animal size. Maximum sprint speed (in lengths per second) scales differently for animals with masses above or below 30 kg [33]; because we were interested in seeing what challenges large animals would face if they moved in similar ways as expected based on trends in small animals, we chose to use the power law relationship for the velocity of animals with masses below 30 kg. We converted velocity to metres per second using the relation between animal mass and length given in [35]:

$$Fr_{max} = \frac{\left(24.21M^{-0.09}\right)\left(0.33M^{0.33}\right)}{\sqrt{9.81\left(0.15M^{0.37}\right)}}$$
$$= \frac{7.99M^{0.24}}{1.22M^{0.19}}$$
$$= 6.56M^{0.06}$$

Substituting our relationship between mass and Froude number at maximum sprint speed into our relationship between Froude number and duty factor gave duty factor $df_{\max}$ at maximum sprint speed:

$$df_{max} = 0.545\left(6.56M^{0.06}\right)^{-0.46}$$
$$= 0.23M^{-0.03}$$

We multiplied stride period by duty factor to find the relationship between mass (in kilograms) and stance duration (in milliseconds) at maximum sprint speed:

$$\text{stance duration}_{\max} = (0.23)(193)M^{0.16-0.03}$$
$$= 44.4\text{M}^{0.13}$$

For a typical 1 kg animal, this relationship indicates that the duration of stance phase will be approximately 44 ms when running at maximum speed. This relationship between stance duration and size is not very sensitive to the assumptions we made about stride frequency conversion from maximum sustained to maximum sprint speed, duty factor in cursorial and non-cursorial animals, maximum sprint speed in animals below and above 30 kg, and animal body length. We tried various permutations of these assumptions, and the coefficient of our final stance duration relationship varied between 39 and 59, while the exponent varied between 0.12 and 0.14.

Confidence intervals for constant component delays

We calculated the 95% confidence interval for each of sensing, synaptic, and neuromuscular junction delays as $t \times \left(sd/\sqrt{n}\right)$, where t is the 95% two-tailed t value with degrees of freedom of n-1, sd is the standard deviation of all data points, and n is the number of data points [36].

Confidence intervals for total delay and relative delay

We used Monte Carlo simulations to estimate the confidence intervals for our total delay and relative delay scaling relationships [37]. These simulations propagated the uncertainty in our component delay relationships, and in previously identified relationships for gait parameters, through our entire calculations. Because our study includes measurements from a total of 12 species ranging from 0.0022 to 3,860 kilograms, we simulated 12 animals whose masses logarithmically spanned the same range. These simulated animals had component delays drawn at random from normal distributions with means derived from each component delay's scaling relationship (table 1); for non-constant delays, the standard deviation of each distribution equalled the standard error of the predicted response (calculated from the associated prediction interval), while for constant delays it equalled the standard error of the mean over all samples. For each simulated animal, we summed their component delays to determine their total delay. We next logarithmically transformed these simulated total delays and used least-squares linear regression to determine the coefficient and exponent of the resulting power law relationship between mass and total delay. We repeated this process 1,000 times, obtaining a distribution of coefficients and a distribution of exponents. Our 95% confidence intervals are the standard deviations of these estimates multiplied by ±1.96, calculated in log space for the coefficient and in linear space for the exponent; we transformed the resulting confidence intervals for the coefficient into linear space. We used the same process to estimate our confidence intervals for our four measures of relative delay, but we divided each simulated animal's total delay by an estimate of their stride duration or stance duration, as appropriate. Each simulated animal's stride duration and stance duration were calculated from movement parameters as described above, but the value of each movement parameter, such as stride frequency, was drawn randomly from a normal distribution with mean and standard deviation calculated from its uncertainty as reported in the literature.

Component delay simulations

To better understand the mechanisms underlying component delays, and to test our assumptions and identified scaling relationships, we simulated the size dependence of key mechanisms involved in synaptic delay, neuromuscular junction delay, electromechanical delay, and force generation delay.

Neurotransmitter diffusion delay

The time required for neurotransmitter molecules to diffuse from the presynaptic neuron to postsynaptic nerve or muscle cell is one contributor to synaptic delay and neuromuscular junction delay. It is not known how the distance between cells scales with animal size, but in mid-sized animals it has been measured to be approximately 0.01—0.02 μm at synapses in the central nervous system [38, 39] and 0.04—0.05 μm at the neuromuscular junction [38]. Using a diffusion coefficient of 7.6×10^{-6} cm^2/s [38], and calculating diffusion time as [39]:

$$\text{diffusion time} = \frac{(\text{diffusion distance})^2}{2\times\text{diffusion coefficient}},$$

these distance ranges would result in a diffusion time of approximately 6.6×10^{-5}—1.6×10^{-3} milliseconds.

Assuming a maximum distance of 0.05 μm between pre- and post-synaptic cells in a 5 kg cat, and conservatively assuming that this distance scales proportional to $M^{1/3}$ in the same way as other linear dimensions such as leg length [10], results in a diffusion distance of about 0.5 μm in a 5,000 kg elephant. This is likely an over-estimate of diffusion distance, because the dimensions of the cells themselves scale less steeply with size [8, 40-42]. Using the same diffusion coefficient as above, this diffusion distance would result in a diffusion time of approximately 0.16 milliseconds for a hypothetical elephant – 100 times slower than that of our hypothetical cat, but still only one-quarter of our average synaptic delay. To account for all our average synaptic delay, the distance between the pre- and post-synaptic cells would need to be 1 μm, which is twice that predicted in the hypothetical cat, and similar to the diameter of the smallest myelinated nerve fibers [43, 44].

Muscle fiber conduction delay

Muscle fiber conduction delay is one contributor to electromechanical delay. To estimate muscle fiber conduction delay and its dependence on animal size, we combined scaling relationships for muscle fiber conduction velocity, muscle fiber diameter, and muscle fiber length. We assumed that muscle fiber conduction velocity (in metres per second) was proportional to the square root of the muscle fiber diameter d (in metres), as in unmyelinated nerve fibers [44, 45]:

$$\text{muscle fiber conduction velocity} \propto d^{1/2}$$

We used an established scaling relationship between animal mass M (in kilograms) and the diameter of fast muscle fibers [46]:

$$d = 60.8 \times 10^{-6} M^{0.007}$$

We combined the scaling relationships for muscle fiber conduction velocity and diameter, and parameterized the resulting power law using the muscle fiber conduction velocity of goats. We chose goats because they are in the middle of the terrestrial mammal size range and because their muscle fiber conduction velocity is known (3 m/s, body mass 23 kg; [13, 47]). This resulted in the scaling relationship between animal mass and muscle fiber conduction velocity of:

$$\begin{aligned}\text{muscle fiber conduction velocity} &= 381(60.8 \times 10^{-6} M^{0.007})^{1/2} \\ &= 2.97 M^{0.0035}\end{aligned}$$

We assumed that muscle fibers are innervated at their midpoint, making the maximum conduction distance half the length of the muscle fiber. We found the scaling relationship for this distance by halving the established scaling relationship between animal mass and muscle fiber length (in millimetres) in the medial gastrocnemius [48]. Then, we divided the result by the muscle fiber conduction velocity scaling relationship to determine how muscle fiber conduction delay (in milliseconds) depends on animal size:

$$\begin{aligned}\text{muscle fiber conduction delay} &= \frac{0.5 \times \text{muscle fiber length}}{\text{muscle fiber conduction velocity}} \\ &= \frac{0.5\left(10.91 M^{0.21}\right)}{2.97 M^{0.0035}} \\ &= 1.84 M^{0.21}\end{aligned}$$

Force generation delay

We used Hill-type muscle models to simulate the dynamics of force generation in different sized animals [49]. Each model consisted of a contractile element (CE), approximating the muscle fibers, in series with an elastic element (SEE), approximating the tendon. Our simulations began with activation of the CE, continued as the CE shortened and stretched the SEE, and ended when the CE ceased shortening because its maximum generated force was balanced by the force in the SEE. The CE has properties that capture the dependence of muscle force on its cross-sectional area, length, velocity, and activation. The SEE force has properties that capture the dependence of tendon force on its cross-sectional area, length, and compliance. The resulting model consisted of two coupled first-order differential equations, with one representing the rate of change of CE activation and the other representing the rate of change of CE length. Because we were interested in isometric contractions of the muscle-tendon unit, we did not require an additional equation for the rate of change of SEE length, but rather this was specified as the difference between the changing CE length and the fixed length of the muscle-tendon unit. Our simulations numerically integrated these equations using Matlab's ode45.m function (MATLAB R2015b, The MathWorks, Inc., Natick, MA, USA). We set the isometric length of the muscle-tendon unit to be the sum of the optimal CE length and the SEE slack length. Thus, the initial condition for CE length was its optimal length. The initial condition for activation was a very low level of activity (2%) equating to a very low level of neural stimulation. Each simulation had a duration of 1 second, with a step increase in neural stimulation to 100% at 0.1 seconds. Following the step increase in neural stimulation, the CE activation began to increase towards its steady state value of 100% activation, causing the CE to shorten and stretch the SEE. The CE eventually stopped shortening because the maximum force that it could generate was balanced by the force in the now stretched SEE. This CE force is the tetanic force, and it was reached well within the 1 second simulation duration for all simulations. For each simulation, we determined the tetanic force generation delay as the time to reach 95% of peak force.

We determined model parameters and their dependence on animal size using a combination of established scaling relationships, and scaling relationships that we determined from reported data (table S8). Below we discuss our rationale for our parameter choices.

Activation time constant: To our knowledge, the dependence of activation dynamics on animal size has not been studied, nor is there sufficient available literature data to reconstruct its scaling relationship; here, we have assumed the activation dynamics to be size-independent. The rate at which a muscle is activated depends upon the rate of calcium release in its muscle fibers, which in turn is dependent on the fibers' density of sarcoplasmic reticulum [50]. There is a trade-off within each muscle fiber between the volume dedicated to sarcoplasmic reticulum and the volume dedicated to the force-generating myofibrils [51, 52]. Maximum isometric stress is size-independent [53, 54], indicating that myofibril density is independent of size. If the density of all other cellular structures, such as mitochondria, also remain constant, the density of sarcoplasmic reticulum would also be size-independent and activation dynamics would not scale with animal size. We tested the sensitivity of our simulations to our assumption of a constant activation time constant – using activation delays that increased with body mass did not strongly affect the predicted scaling of tetanic force generation delay.

CE maximum isometric force: We determined this parameter as the product of maximum isometric muscle stress (which is size-independent) and muscle fiber cross-sectional area (which is size-dependent). Maximum isometric stress is relatively constant for all animal sizes, at about 0.25 MPa, while muscle fiber area (in millimetres^2) in the gastrocnemius scales as $304.2M^{0.77}$ [48].

CE optimal (rest) length: We assumed that this parameter was equal to the resting length of muscle fibers, and used the measured gastrocnemius muscle fiber length scaling relationship [48].

CE force-length width parameter: This parameter specifies the maximum amount of shortening that the CE can undergo and still generate force [49]. We used the value provided by van den Bogert [49], and assumed it was independent of body size because sarcomere length remains relatively similar across species [55].

CE maximum shortening velocity: There have been several efforts to identify the scaling relationship for muscle's maximum shortening velocity [46, 56, 57]. We chose to use the scaling relationship for maximum shortening velocity of fast-twitch fibers established by Seow et al. [46] because this study uses data measured from the same muscle using consistent methods in a wide size range of animals, and focuses on fast-twitch muscle speed independent of slow-twitch muscle; we corrected the scaling relationship to 38°C using a Q_{10} of 2.23 [58].

CE force-velocity shape parameter: This parameter determines the curvature of the hyperbolic force-velocity relationship. We used an intermediate value of 0.20 [59], and assumed that this value was size-independent.

SEE slack (rest) length: We assumed that this parameter was equal to the resting length of the tendon, and used an established gastrocnemius tendon length scaling relationship [48].

SEE stiffness: We determined the scaling of this parameter as the product of tendon elastic modulus and tendon cross-sectional area divided by tendon resting length; we used established gastrocnemius-specific scaling relationships for each of these variables [48].

We used the above parameters to simulate the dynamics of force generation at 12 logarithmically-spaced body masses spanning the entire size range of terrestrial mammals from our measurements – 0.0022 to 3,860 kilograms. We then used least-squares linear regression of logarithmically transformed species delays and masses to determine the power law relationship between body mass and the predicted time to peak tetanic force:

$$\text{tetanic delay} = 94.2M^{0.24}$$

Consistent with previous findings, our simulated tetanic delays are about 5 times longer than the time to peak twitch force [60].

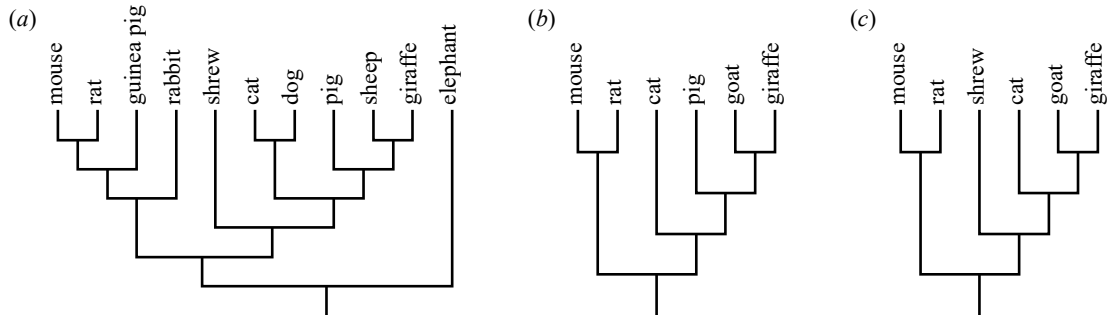

Figure S1. Trees for phylogenetically independent contrasts analyses. We used tree (*a*) for nerve conduction delay, (*b*) for electromechanical delay, and (*c*) for force generation delay. All trees had branch lengths equal to one.

Table S1. Sensing delays and animal masses.

Species	**N**	**Mass (kg)**	**Mass sd (kg)**	**Delay (ms)**	**Delay sd (ms)**	**Muscle**	**Ref.**
Cat	5			1	0.35*	Quad	[2]
	1			0.25	0.025*	MG	[61]
	1	2.75	0.13*	0.6 †		Ext	[3]
Mean		**2.75**		**0.62**			

Standard deviations (sd) approximated by dividing the range by four are indicated with a superscript *, values obtained from figures are indicated with a superscript †. Muscles are Ext = ankle extensor, MG = medial gastrocnemius, Quad = quadriceps.

Table S2. Nerve conduction delays and animal masses.

Species	N	Mass (kg)	Mass sd (kg)	CV (m/s)	CV sd (m/s)	Delay (ms)	Nerve	Type	Ref.
Shrew	6	0.0057	0.0007	42.1	6.3		Sc	M	[8]
Mean		**0.0057**		42.1		**1.40**			
Mouse	18	0.023	0.001*	58.1†	1.5†		Sc/T	S	[62]
	18	0.023	0.001*	41.4†	0.8†		Sc/T	M	[62]
	6	0.025	0.003*	43.2	0.6		Sc/T	M	[63]
	8	0.031‡		62.9	5.7		Sc/T	M	[64]
	9	0.031‡		49.6	4.6		Sc/T	M	[64]
	8	0.031‡		52.4	4.6		Sc/T	M	[64]
	6	0.031‡		49.7	5.2		Sc/T	M	[64]
	11	0.031	0.002	59.8			Sc	C	[65]
	12			20	4†		Sc	M	[66]
	58	0.0225	0.001*	76.5	8.3		Sc	M	[67]
Mean		**0.027**		51.4		**2.18**			
Rat	19	0.43	0.03*	68.7	10.0		Sc	M	[68]
	20	0.19	0.01*	55.5	2.9		Sc/T	M	[69]
	6	0.325	0.028*	54.7†	2.8†		Sc/T	S	[70]
	12	0.227	0.025	69.4			Sc	C	[65]
	10	0.516	0.026	54.6	2.5		Sc/T	M	[71]
	20	0.575	0.043*	53.3	2.7		Sc/T	M	[72]
Mean		**0.377**		59.4		**4.01**			
Guinea pig	29	0.662‡		74.6†	9.0†		Sc	M	[73]
	12			73.6	3.4		Sc/T	S	[74]
	12			74.5	2.4		Sc/T	M	[74]
	10	0.75	0.08	80.8			Sc	C	[65]
Mean		**0.71**		76.0		**3.87**			
Rabbit	10	3.25	0.38*	70.8	3.1		Sc	M	[75]
	12	3.25	0.13*	55	6.9		Sc/T	M	[76]
	2	3		57.3†	11.2†		Sc	M	[77]
	14	2		59	4.8		Sc/T	M	[72]
Mean		**2.88**		60.5		**7.76**			
Cat	14	4.4	0.6*	101.4	12.9		Sc/T	M	[78]
	20			80.2	7.9		T	S	[79]
	20			91.0	6.5*		Sc/T	M	[80]
	25	4.1	0.65*	99.4	8.5		Sc/T	M	[81]
Mean		**4.3**		93.0		**5.78**			
Dog	6	17.5	4.8*	74	17.3		Sc/T	S	[82]
	5			66	4.3		Sc/T	C	[83]
	19	22.7	6.8*	68.3	4.2		Sc/T	M	[84]
	7			89.2	12.4		Sc/T	M	[85]
	28—56			62.9	2.3§		Sc/T	M	[86]
	10	11.7		68.2	1.4		Sc/T	M	[87]
Mean		**17.3**		71.4		**12.0**			
Pig	14	20.2	6.3	77.7	16.5		Sc	S	[88]
Mean		**20.2**		77.7		**11.5**			
Sheep	3	97.5‡		96.3	3		Sc/T	M	[89]
	15	97.5‡		98.6	13.1		Sc/T	M	[85]
Mean		**97.5**		97.45		**15.5**			
Giraffe	4	466.5	20.0	50.4	20.0		T	M	[9]
Mean		**466.5**		50.4		**50.5**			
Elephant	1	3860		70			T	S	[8]
Mean		**3860**		70		**73.4**			

Standard deviations (sd) approximated by dividing the range by four are indicated with a superscript *, values obtained from figures are indicated with a superscript †, masses estimated from other sources (e.g. species growth charts) are indicated with a superscript ‡, standard errors are indicated with a superscript §. Nerves are Sc = sciatic, T = tibial. Conduction velocity (CV) types are M = motor, S = sensory, C = combined motor and sensory.

Table S3. Synaptic delays and animal masses.

Species	N	Mass (kg)	Mass sd (kg)	Delay (ms)	Delay sd (ms)	Level	Muscle	Ref.
Mouse	28	0.022	0.002*	1.3		L4—L6		[90]
	1	0.025		0.79†			T	[91]
		0.0275	0.0038*	0.62	0.13§	L4—L5	T	[92]
Mean		**0.025**		**0.90**				
Rat	4	0.45	0.015*	1.14		L5	FHL	[93, 94]
Mean		**0.45**		**1.14**				
Cat				0.6		L6—S1		[95]
	1			0.54†			MG	[96]
	5			0.54		L7—S1		[97]
				0.90†	0.07†	L7—S1	Tri	[98]
				0.6		S1	MG	[61]
				0.8	0.1*		MG	[99]
				0.65	0.08*		MG	[100]
	12			0.37	0.15	L6—S1	MG	[101, 102]
	21	2.25	0.375*	0.46	0.01	L6—S1	MG	[103, 104]
	5			0.81	0.09	L7—S1		[105]
	8			0.8	0.05*	L6—S2	MG/Sol	[106]
				0.47	0.02§		MG	[107]
		3.9	1.05*	0.4	0.13*	L7—S1		[108]
Mean		**3.08**		**0.61**				
Dog		18		0.6		L5—L6		[8, 109]
Mean		**18**		**0.6**				

Standard deviations (sd) approximated by dividing the range by four are indicated with a superscript *, values obtained from figures are indicated with a superscript †, standard errors are indicated with a superscript §. Levels are spinal root levels L = lumbar, S = sacral. Muscles supplied by at least one neuron of the synapse are FHL = flexor hallucis longus, MG = medial gastrocnemius, Sol = soleus, T = tibial, Tri = triceps surae. Where two references are given, one gives the delay and one gives the mass, with the exception of [102] which gives the level.

Table S4. Neuromuscular junction delays and animal masses.

Species	N	Mass (kg)	Mass sd (kg)	Delay (ms)	Delay sd (ms)	Muscle	Ref.
Mouse	58	0.0225	0.0013*	0.68		G	[67]
Mean		**0.0225**		**0.68**			
Cat	5			0.6	0.025*	PT	[4]
	1	2.03	0.38	1.1†		FDL / FHL	[5]
Mean		**2.03**		**0.9**			
Dog	9	18.0		0.7		G	[8, 110]
Mean		**18.0**		**0.7**			
Pig	11	19.6	5.9	1.27	0.25	G	[88]
Mean		**19.6**		**1.27**			

Standard deviations (sd) approximated by dividing the range by four are indicated with a superscript *, values obtained from figures are indicated with a superscript †. Muscles are G = gastrocnemius, FDL = flexor digitorum longus, FHL = flexor hallucis longus, PT = peroneus tertius. Where two references are given, one the delay and one gives the mass.

Table S5. Electromechanical delays and animal masses.

Species	N	Mass (kg)	Mass sd (kg)	Delay (ms)	Delay sd (ms)	Muscle	Type	Ref.
Mouse	1	0.028‡		1.9†		Tri	F	[111]
Mean		**0.028**		**1.9**				
Rat	26	0.38	0.05*	4.63	0.6	MG	F	[112]
	1	0.377		4.5		MG	Mix	[8, 9]
	5	0.295	0.023*	3.78	0.42	MG	FF	[113]
	3			1.19†		G	Mix	[114]
Mean		**0.351**		**3.52**				
Cat	1	2.65	0.3*	5.2†		LG	FF	[6]
	1	3.5	0.35*	4.00†		G	F	[115, 116]
Mean		**3.08**		**4.59**				
Pig	11	19.6	5.9	9.91	1.07	G	Mix	[88]
Mean		**19.6**		**9.91**				
Goat	5	23	3.5	10.5		MG	F	this study, [13]
Mean		**23**		**10.5**				
Giraffe	4	498.75	83.18	13.4	1.4	MG	Mix	[9]
Mean		**498.75**		**13.4**				

Standard deviations (sd) approximated by dividing the range by four are indicated with a superscript *, values obtained from figures are indicated with a superscript †, masses estimated from species growth charts are indicated with a superscript ‡. Muscles are G = gastrocnemius, LG = lateral gastrocnemius, MG = medial gastrocnemius, Tri = triceps surae. Muscle fiber types are F = fast, FF = fast fatiguable, Mix = both fast and slow. Where two references are given, one gives the delay and one gives the mass.

Table S6. Force generation delays and animal masses.

Species	N	Mass (kg)	Mass sd (kg)	Delay (ms)	Delay sd (ms)	Muscle	Type	Ref.
Shrew	6	0.0022	0.0003	3.7		EDL	F	[7]
Mean		**0.0022**		**3.7**				
Mouse	1	0.028‡		12†		Tri	F	[111]
Mean		**0.028**		**12**				
Rat	24	0.28	0.035*	15.5	2	MG	F	[117]
	26	0.38	0.05*	14.92	1.59	MG	F	[112]
	4	0.295	0.023*	11.8	1.6	MG	FF	[118]
	15	0.38	0.116	13.4	2.1	MG	FF	[119]
	5	0.39	0.023	12.2	1.8	MG	FF	[120]
	5	0.295	0.023*	13.35	1.4	MG	FF	[113]
Mean		**0.34**		**13.5**				
Cat		2.5	0.25*	22	3.5*	MG/G	F	[121]
	8			20.1†	4.9†	MG	F	[122]
	1	2.7	0.3*	23.6†		LG	FF	[6]
	1	3.1	0.1*	34.9†	2.5†	MG	F	[123]
		3.5	0.65*	27.5	5.1	MG	FF	[124]
	1			17.9†		MG	FF	[125]
	4	3.1	0.04*	26.1	5.3	MG	FF	[118]
	7	2.80	0.61	32.2	6.8	MG	FF	[119]
	3	3.4	0.27	35.1	5.4	MG	FF	[120]
	1	3.5	0.5*	34.4†		MG	F	[126]
	1	3.5	0.5*	36.8†		MG	FF	[1]
	1	3.5‡	0.35*	23.8†		G	F	[115, 116]
Mean		**3.2**		**27.9**				
Goat	7	23	3.5	36.7		MG, LG	F	[13]
Mean		**23**		**36.7**				
Giraffe	4	498.75	83.18	45.9	10.7	MG	Sup	[9]
Mean		**498.75**		**45.9**				

Standard deviations (sd) approximated by dividing the range by four are indicated with a superscript *, values obtained from figures are indicated with a superscript †, masses estimated from other sources (e.g. species growth charts) are indicated with a superscript ‡. Muscles are EDL = extensor digitorum longus, G = gastrocnemius LG = lateral gastrocnemius, MG = medial gastrocnemius, Tri = triceps surae. Muscle fiber types are F = fast, FF = fast fatiguable, Sup = superficial fibers (generally faster; [14-16]).

Table S7. Phylogenetically independent contrasts analyses

Delay	**Pearson product-moment correlation**	**Least squares regression**		***p***
		slope	R^2	
Nerve conduction	0.97	0.30	0.93	<0.001
Electromechanical	0.91	0.19	0.83	0.01
Force generation	0.92	0.20	0.85	<0.01

Trees are shown in figure S1. Analyses were performed on contrasts of the logarithmically transformed species averages shown in tables S2, S5, and S6.

Table S8. Model parameters for simulating force generation delay.

Parameter	**Value**	**Unit**	**Ref.**
Activation time constant	0.005	s	[127, 128]
Contractile element (CE)			
Maximum isometric force	$60.8\ M^{0.77}$	N	[48]
Optimal (rest) length	$10.9\ M^{0.21}$	mm	[48]
Force-length width parameter	0.63	[dimensionless]	[49]
Maximum shortening velocity	$1.49\ M^{-0.126}$	CE resting lengths·s^{-1}	[46]
Series elastic element (SEE)			
Slack (rest) length	$63.7\ M^{0.34}$	mm	[48]
Stiffness	$56.9\ M^{0.34}$	N·mm^{-1}	[48]

REFERENCES

[1] Proske, U. & Waite, P.M. 1974 Properties of types of motor units in the medial gastrochemius muscle of the cat. *Brain Res.* **67**, 89-101.
[2] Jolly, W.A. 1910 On the latency of sensory nerve endings to mechanical stimulation. *J Physiol* **41**, 14-15.
[3] Prochazka, A., Westerman, R.A. & Ziccone, S.P. 1976 Discharges of single hindlimb afferents in the freely moving cat. *J. Neurophysiol.* **39**, 1090-1104.
[4] Eccles, J.C. & O'Connor, W.J. 1939 Responses which nerve impulses evoke in mammalian striated muscles. *J. Physiol.* **97**, 44-102.
[5] Knott, S., Lewis, D.M. & Luck, J.C. 1971 Motor unit areas in a cat limb muscle. *Exp. Neurol.* **30**, 475-483.
[6] Burke, R.E., Levine, D.N., Tsairis, P. & Zajac, F. 1973 Physiological types and histochemical profiles in motor units of the cat gastrocnemius. *J. Physiol.* **234**, 723-748.
[7] Peters, T., Kubis, H.P., Wetzel, P., Sender, S., Asmussen, G., Fons, R. & Jurgens, K.D. 1999 Contraction parameters, myosin composition and metabolic enzymes of the skeletal muscles of the etruscan shrew *Suncus etruscus* and of the common European white-toothed shrew *Crocidura russula* (Insectivora: soricidae). *J. Exp. Biol.* **202**, 2461-2473.
[8] More, H.L., Hutchinson, J.R., Collins, D.F., Weber, D.J., Aung, S.K.H. & Donelan, J.M. 2010 Scaling of sensorimotor control in terrestrial mammals. *Proc. Biol. Sci.* **277**, 3563-3568.
[9] More, H.L., O'Connor, S.M., Brøndum, E., Wang, T., Bertelsen, M.F., Grøndahl, C., Kastberg, K., Hørlyck, A., Funder, J. & Donelan, J.M. 2013 Sensorimotor responsiveness and resolution in the giraffe. *J. Exp. Biol.* **216**, 1003-1011.
[10] Alexander, R.M., Jayes, A.S., Maloiy, G.M.O. & Wathuta, E.M. 1979 Allometry of the limb bones of mammals from shrews (*Sorex*) to elephant (*Loxodonta*). *J. Zool. Lond.* **189**, 305-314.
[11] Burke, R.E., Strick, P.L., Kanda, K., Kim, C.C. & Walmsley, B. 1977 Anatomy of medial gastrocnemius and soleus motor nuclei in cat spinal cord. *J. Neurophysiol.* **40**, 667-680.
[12] Hashizume, K., Kanda, K. & Burke, R.E. 1988 Medial gastrocnemius motor nucleus in the rat: age-related changes in the number and size of motoneurons. *J. Comp. Neurol.* **269**, 425-430.
[13] Lee, S.S., Miara M, d., B., Arnold, A.S., Biewener, A.A. & Wakeling, J.M. 2011 EMG analysis tuned for determining the timing and level of activation in different motor units. *J. Electromyogr. Kinesiol.* **21**, 557-565.
[14] Roy, R.R., Graham, S. & Peterson, J.A. 1988 Fiber type composition of the plantarflexors of giraffes (*Giraffa camelopardalis*) at different postnatal stages of development. *Comp. Biochem. Physiol. A* **91**, 347-352.
[15] Roy, R.R., Talmadge, R.J., Hodgson, J.A., Oishi, Y., Baldwin, K.M. & Edgerton, V.R. 1999 Differential response of fast hindlimb extensor and flexor muscles to exercise in adult spinalized cats. *Muscle Nerve* **22**, 230-241.
[16] Wang, L.C. & Kernell, D. 2001 Fibre type regionalisation in lower hindlimb muscles of rabbit, rat and mouse: a comparative study. *J. Anat.* **199**, 631-643.
[17] Gingerich, P.D. 2000 Arithmetic or geometric normality of biological variation: an empirical test of theory. *J. Theor. Biol.* **204**, 201-221.
[18] Kerkhoff, A.J. & Enquist, B.J. 2009 Multiplicative by nature: Why logarithmic transformation is necessary in allometry. *J. Theor. Biol.* **257**, 519-521.
[19] Packard, G.C. 2009 On the use of logarithmic transformations in allometric analyses. *J. Theor. Biol.* **257**, 515-518; discussion 519-521.
[20] Felsenstein, J. 1985 Phylogenies and the Comparative Method. *Am. Nat.* **125**, 1-15.

[21] Maddison, W.P. & Maddison, D.R. 2015 Mesquite: a modular system for evolutionary analysis.
[22] Bininda-Emonds, O.R.P., Cardillo, M., Jones, K.E., MacPhee, R.D.E., Beck, R.M.D., Grenyer, R., Price, S.A., Vos, R.A., Gittleman, J.L. & Purvis, A. 2007 The delayed rise of present-day mammals. *Nature* **446**, 507-512.
[23] Meredith, R.W., Janečka, J.E., Gatesy, J., Ryder, O.A., Fisher, C.A., Teeling, E.C., Goodbla, A., Eizirik, E., Simão, T.L.L., Stadler, T., et al. 2011 Impacts of the Cretaceous Terrestrial Revolution and KPg extinction on mammal diversification. *Science* **334**, 521-524.
[24] Welker, F., Collins, M.J., Thomas, J.A., Wadsley, M., Brace, S., Cappellini, E., Turvey, S.T., Reguero, M., Gelfo, J.N., Kramarz, A., et al. 2015 Ancient proteins resolve the evolutionary history of Darwin's South American ungulates. *Nature*.
[25] Ackerly, D.D. 2000 Taxon sampling, correlated evolution, and independent contrasts. *Evolution* **54**, 1480-1492.
[26] Martins, E.P. & Garland, J., Theodore. 1991 Phylogenetic analyses of the correlated evolution of continuous characters: A simulation study. *Evolution* **45**, 534-557.
[27] Midford, P.E., Garland, T.J. & Maddison, W.P. 2005 PDAP package of Mesquite. Version 1.07.
[28] Heglund, N.C., Taylor, C.R. & McMahon, T.A. 1974 Scaling stride frequency and gait to animal size: mice to horses. *Science* **186**, 1112-1113.
[29] Biewener, A.A. 1983 Allometry of quadrupedal locomotion: the scaling of duty factor, bone curvature and limb orientation to body size. *J. Exp. Biol.* **105**, 147-171.
[30] Heglund, N.C. & Taylor, C.R. 1988 Speed, stride frequency and energy cost per stride: how do they change with body size and gait? *J. Exp. Biol.* **138**, 301-318.
[31] Garland, T. 1983 The relation between maximal running speed and body mass in terrestrial mammals. *J. Zool. Lond.* **199**, 157-170.
[32] Alexander, R.M. & Jayes, A.S. 1983 A dynamic similarity hypothesis for the gaits of quadrupedal mammals. *J. Zool. Lond.* **201**, 135-152.
[33] Iriarte-Díaz, J. 2002 Differential scaling of locomotor performance in small and large terrestrial mammals. *J. Exp. Biol.* **205**, 2897-2908.
[34] Kilbourne, B.M. & Hoffman, L.C. 2013 Scale effects between body size and limb design in quadrupedal mammals. *PLoS One* **8**, e78392.
[35] Silva, M. 1998 Allometric scaling of body length: Elastic or geometric similarity in mammalian design. *J. Mammal.* **79**, 20-32.
[36] Schwarz, C.J. 2009 Sampling, Regression, Experimental Design and Analysis for Environmental Scientists, Biologists, and Resource Managers. Department of Statistics and Actuarial Science, Simon Fraser University.
[37] Press, W.H., Teukolsky, S.A., Vetterling, W.T. & Flannery, B.P. 2007 *Numerical Recipes: The Art of Scientific Computing*. 3rd ed. Cambridge, NY, Cambridge University Press.
[38] Eccles, J.C. & Jaeger, J.C. 1958 The relationship between the mode of operation and the dimensions of the junctional regions at synapses and motor end-organs. *Proc. Biol. Sci.* **148**, 38-56.
[39] Sabatini, B.L. & Regehr, W.G. 1999 Timing of synaptic transmission. *Annu. Rev. Physiol.* **61**, 521-542.
[40] Changizi, M.A. 2001 Principles underlying mammalian neocortical scaling. *Biol. Cybern.* **84**, 207-215.
[41] Phalen, G. & Davenport, H.A. 1937 Pericellular end-bulbs in the central nervous system of vertebrates. *J. Comp. Neurol.* **68**, 67-81.

[42] Savage, V.M., Allen, A.P., Brown, J.H., Gillooly, J.F., Herman, A.B., Woodruff, W.H. & West, G.B. 2007 Scaling of number, size, and metabolic rate of cells with body size in mammals. *Proc. Natl. Acad. Sci. USA* **104**, 4718-4723.
[43] Duncan, D. 1934 A relation between axone diameter and myelination determined by measurement of myelinated spinal root fibers. *J. Comp. Neurol.* **60**, 437-431.
[44] Rushton, W.A.H. 1951 A theory of the effects of fibre size in medullated nerve. *J. Physiol.* **115**, 101-122.
[45] Loeb, G.E., Pratt, C.A., Chanaud, C.M. & Richmond, F.J.R. 1987 Distribution and innervation of short, interdigitated muscle fibers in parallel-fibered muscles of the cat hindlimb. *J. Morphol.* **191**, 1-15.
[46] Seow, C.Y. & Ford, L.E. 1991 Shortening velocity and power output of skinned muscle fibers from mammals having a 25,000-fold range of body mass. *J. Gen. Physiol.* **97**, 541-560.
[47] Gans, C., Loeb, G.E. & de Vree, F. 1989 Architecture and consequent physiological properties of the semitendinosus muscle in domestic goats. *J. Morphol.* **199**, 287-297.
[48] Pollock, C.M. & Shadwick, R.E. 1994 Allometry of muscle, tendon, and elastic energy storage capacity in mammals. *Am. J. Physiol.* **266**, R1022-1031.
[49] van den Bogert, A.J. & Nigg, B.M. 2007 Simulation In *Biomechanics of the musculo-skeletal system* (eds. B.M. Nigg & W. Herzog), pp. xiii, 672 p., 3rd ed. New Jersey, John Wiley & Sons.
[50] Rome, L.C. 2006 Design and function of superfast muscles: new insights into the physiology of skeletal muscle. *Annu. Rev. Physiol.* **68**, 193-221.
[51] Lindstedt, S.L., McGlothlin, T., Percy, E. & Pifer, J. 1998 Task-specific design of skeletal muscle: balancing muscle structural composition. *Comp. Biochem. Physiol. B* **120**, 35-40.
[52] Rome, L.C. & Lindstedt, S.L. 1998 The Quest for Speed: Muscles Built for High-Frequency Contractions. *News Physiol. Sci.* **13**, 261-268.
[53] Close, R.I. 1972 Dynamic Properties of Mammalian Skeletal-Muscles. *Physiol. Rev.* **52**, 129-197.
[54] Wells, J.B. 1965 Comparison of Mechanical Properties between Slow and Fast Mammalian Muscles. *J. Physiol. (London)* **178**, 252-269.
[55] Burkholder, T.J. & Lieber, R.L. 2001 Sarcomere length operating range of vertebrate muscles during movement. *J. Exp. Biol.* **204**, 1529-1536.
[56] Marx, J.O., Olsson, M.C. & Larsson, L. 2006 Scaling of skeletal muscle shortening velocity in mammals representing a 100,000-fold difference in body size. *Pflug. Arch. Eur. J. Phy.* **452**, 222-230.
[57] Rome, L.C., Sosnicki, A.A. & Goble, D.O. 1990 Maximum velocity of shortening of three fibre types from horse soleus muscle: implications for scaling with body size. *J. Physiol.* **431**, 173-185.
[58] Stein, R.B., Gordon, T. & Shriver, J. 1982 Temperature dependence of mammalian muscle contractions and ATPase activities. *Biophys. J.* **40**, 97-107.
[59] McMahon, T.A. 1984 *Muscles, reflexes, and locomotion*. Princeton, N.J., Princeton University Press.
[60] Close, R. 1964 Dynamic Properties of Fast and Slow Skeletal Muscles of the Rat during Development. *J. Physiol. (Lond.)* **173**, 74-95.
[61] Lloyd, D.P.C. 1943 Conduction and synaptic transmission of the reflex response to stretch in spinal cats. *J. Neurophysiol.* **6**, 317-326.
[62] Higashimori, H., Whetzel, T.P., Mahmood, T. & Carlsen, R.C. 2005 Peripheral axon caliber and conduction velocity are decreased after burn injury in mice. *Muscle Nerve* **31**, 610-620.

[63] Kennedy, J.M. & Zochodne, D.W. 2000 The regenerative deficit of peripheral nerves in experimental diabetes: its extent, timing and possible mechanisms. *Brain* **123**, 2118-2129.
[64] Oh, S.S., Hayes, J.M., Sims-Robinson, C., Sullivan, K.A. & Feldman, E.L. 2010 The effects of anesthesia on measures of nerve conduction velocity in male C57B16/J mice. *Neurosci. Lett.* **483**, 127-131.
[65] Schnepp, G., Schnepp, P. & Spaan, G. 1971 [Analysis of peripheral nerve fibres in animals of different body size. I. Total fibre count, fibre size, and nerve conduction velocity]. *Z. Zellforsch. Mikrosk. Anat.* **119**, 77-98.
[66] Schulz, A., Walther, C., Morrison, H. & Bauer, R. 2014 In vivo electrophysiological measurements on mouse sciatic nerves. *J. Vis. Exp.: JoVE*. **86**, e51181.
[67] Xia, R.H., Yosef, N. & Ubogu, E.E. 2010 Dorsal caudal tail and sciatic motor nerve conduction studies in adult mice: technical aspects and normative data. *Muscle Nerve* **41**, 850-856.
[68] Cameron, N.E., Cotter, M.A. & Robertson, S. 1989 The effect of aldose reductase inhibition on the pattern of nerve conduction deficits in diabetic rats. *Q. J. Exp. Physiol.* **74**, 917-926.
[69] Landegren, T., Risling, M., Brage, A. & Persson, J.K.E. 2006 Long-term results of peripheral nerve repair: a comparison of nerve anastomosis with ethyl-cyanoacrylate and epineural sutures. *Scand. J. Plast. Reconstr. Surg. Hand Surg.* **40**, 65-72.
[70] Patel, J. & Tomlinson, D.R. 1999 Nerve conduction impairment in experimental diabetes-proximodistal gradient of severity. *Muscle Nerve* **22**, 1403-1411.
[71] Shibata, T., Naruse, K., Kamiya, H., Kozakae, M., Kondo, M., Yasuda, Y., Nakamura, N., Ota, K., Tosaki, T., Matsuki, T., et al. 2008 Transplantation of bone marrow-derived mesenchymal stem cells improves diabetic polyneuropathy in rats. *Diabetes* **57**, 3099-3107.
[72] Thomas, P.K., Jefferys, J.G., Sharma, A.K. & Bajada, S. 1981 Nerve conduction velocity in experimental diabetes in the rat and rabbit. *J. Neurol. Neurosurg. Psychiatry* **44**, 233-238.
[73] Chau, C.H., Shum, D.K., Chan, Y.S. & So, K.F. 1999 Heparan sulphates upregulate regeneration of transected sciatic nerves of adult guinea-pigs. *Eur. J. Neurosci.* **11**, 1914-1926.
[74] Hall, J.I. 1967 Studies on demyelinated peripheral nerves in guinea-pigs with experimental allergic neuritis. A histological and electrophysiological study. II. Electrophysiological observations. *Brain* **90**, 313-332.
[75] Harvey, G.K., Pollard, J.D., Schindhelm, K. & Antony, J. 1987 Chronic experimental allergic neuritis. An electrophysiological and histological study in the rabbit. *J. Neurol. Sci.* **81**, 215-225.
[76] Mani, G.V., Shurey, C. & Green, C.J. 1992 Is early vascularization of nerve grafts necessary? *J. Hand. Surg. Brit. Eur.* **17**, 536-543.
[77] Suzuki, Y. & Shirai, Y. 2003 Motor nerve conduction analysis of double crush syndrome in a rabbit model. *J. Orthop. Sci.* **8**, 69-74.
[78] Malik, R. & Ho, S. 1989 Motor nerve conduction parameters in the cat. *J. Small Anim. Pract.* **30**, 396-400.
[79] Redding, R.W. & Ingram, J.T. 1984 Sensory nerve conduction velocity of cutaneous afferents of the radial, ulnar, peroneal, and tibial nerves of the cat: reference values. *Am. J. Vet. Res.* **45**, 1042-1045.
[80] Ribelin, W.E. & Leswing, R.J. 1968 Nerve conduction in cats and *Cebus albifrons* monkeys. *Am. J. Vet. Res.* **29**, 2401-2405.
[81] Picavet, P.M. & Lambillon, D.E. 1993 Motor nerve conduction in the cat's hind limb. *Prog. Vet. Neurol.* **4**, 121-125.

[82] Knecht, C.D., Redding, R. & Hyams, D. 1983 Stimulation techniques and response characteristics of the M and F waves and H reflex in dogs. *Vet. Res. Commun.* **6**, 123-132.
[83] Lee, A.F. & Bowen, J.M. 1970 Evaluation of motor nerve conduction velocity in the dog. *Am. J. Vet. Res.* **31**, 1361-1366.
[84] Malik, R., Ho, S. & Church, D. 1989 A new method for recording and analysing evoked motor potentials from dogs. *J. Small Anim. Pract.* **30**, 13-19.
[85] Steiss, J.E. & Argue, C.K. 1987 Normal values for radial, peroneal and tibial motor nerve conduction velocities in adult sheep, with comparison to adult dogs. *Vet. Res. Commun.* **11**, 243-252.
[86] Swallow, J.S. & Griffiths, I.R. 1977 Age related changes in the motor nerve conduction velocity in dogs. *Res. Vet. Sci.* **23**, 29-32.
[87] Walker, T.L., Redding, R.W. & Braund, K.G. 1979 Motor nerve conduction velocity and latency in the dog. *Am. J. Vet. Res.* **40**, 1433-1439.
[88] Szentkuti, L., Schlegel, O. & Sallai, J. 1990 Neuromuscular transmission in the gastrocnemius muscle of young domestic and wild pigs. *Zentralbl. Veterinarmed. A* **37**, 339-347.
[89] Loke, J.C., Harding, R. & Proske, U. 1986 Conduction velocity in peripheral nerve of foetal, newborn and adult sheep. *Neurosci. Lett.* **71**, 317-322.
[90] Huizar, P., Kuno, M. & Miyata, Y. 1975 Electrophysiological properties of spinal motoneurones of normal and dystrophic mice. *J Physiol* **248**, 231-246.
[91] Meehan, C.F., Sukiasyan, N., Zhang, M., Nielsen, J.B. & Hultborn, H. 2010 Intrinsic properties of mouse lumbar motoneurons revealed by intracellular recording in vivo. *J. Neurophysiol.* **103**, 2599-2610.
[92] Schomburg, E.D., Kalezic, I., Dibaj, P. & Steffens, H. 2013 Reflex transmission to lumbar alpha-motoneurones in the mouse similar and different to those in the cat. *Neurosci. Res.* **76**, 133-140.
[93] Wayner, J., M. J. & Emmers, R. 1958 Spinal synaptic delay in young and aged rats. *Am. J. Physiol.* **194**, 403-405.
[94] Emmers, R. 1959 The effects of brain-stem stimulation on hind-leg movements in the hooded rat. *Exp. Neurol.* **1**, 171-186.
[95] Brock, L.G., Coombs, J.S. & Eccles, J.C. 1952 The recording of potentials from motoneurones with an intracellular electrode. *J. Physiol.* **117**, 431-460.
[96] Eccles, J.C., Eccles, R.M. & Lundberg, A. 1957 The convergence of monosynaptic excitatory afferents on to many different species of alpha motoneurones. *J. Physiol.* **137**, 22-50.
[97] Eide, E., Lundberg, A. & Voorhoeve, P. 1961 Monosynaptically evoked inhibitory post-synaptic potentials in motoneurones. *Acta Physiol. Scand.* **53**, 185-195.
[98] Kuno, M. & Miyahara, J.T. 1969 Non-linear summation of unit synaptic potentials in spinal motoneurones of the cat. *J. Physiol.* **201**, 465-477.
[99] Mendell, L.M. & Henneman, E. 1968 Terminals of single Ia fibers: distribution within a pool of 300 homonymous motor neurons. *Science* **160**, 96-98.
[100] Mendell, L.M. & Henneman, E. 1971 Terminals of single Ia fibers: location, density, and distribution within a pool of 300 homonymous motoneurons. *J. Neurophysiol.* **34**, 171-187.
[101] Munson, J.B. & Sypert, G.W. 1978 Latency-rise time relationship in unitary postsynaptic potentials. *Brain Res.* **151**, 404-408.
[102] Scott, J.G. & Mendell, L.M. 1976 Individual EPSPs produced by single triceps surae Ia afferent fibers in homonymous and heteronymous motoneurons. *J. Neurophysiol.* **39**, 679-692.

[103] Munson, J.B. & Sypert, G.W. 1979 Properties of single fibre excitatory post-synaptic potentials in triceps surae motoneurones. *J. Physiol.* **296**, 329-342.
[104] Munson, J.B. & Sypert, G.W. 1979 Properties of single central Ia afferent fibres projecting to motoneurones. *J. Physiol.* **296**, 315-327.
[105] Renshaw, B. 1940 Activity in the simplest spinal reflex pathways. *J. Neurophysiol.* **3**, 373-387.
[106] Stuart, D.G., Willis, W.D., Jr. & Reinking, R.M. 1971 Stretch-evoked excitatory postsynaptic potentials in motoneurons. *Brain Res.* **33**, 115-125.
[107] Sypert, G.W., Fleshman, J.W. & Munson, J.B. 1980 Comparison of monosynaptic actions of medial gastrocnemius group Ia and group II muscle spindle afferents on triceps surae motoneurons. *J. Neurophysiol.* **44**, 726-738.
[108] Watt, D.G., Stauffer, E.K., Taylor, A., Reinking, R.M. & Stuart, D.G. 1976 Analysis of muscle receptor connections by spike-triggered averaging. 1. Spindle primary and tendon organ afferents. *J. Neurophysiol.* **39**, 1375-1392.
[109] Rosenblueth, A., Wiener, N., Pitts, W. & García Ramos, J. 1949 A statistical analysis of synaptic excitation. *J. Cell. Compar. Physl.* **34**, 173-205.
[110] Adzhimolaev, T.A. 1965 Characteristics of synaptic delay in the neuromuscular apparatus of dogs of various ages. *Bull. Exp. Biol. Med.* **59**, 483-485.
[111] Manuel, M. & Heckman, C.J. 2011 Adult mouse motor units develop almost all of their force in the subprimary range: a new all-or-none strategy for force recruitment? *J. Neurosci.* **31**, 15188-15194.
[112] Grottel, K. & Celichowski, J. 1988 Contraction time and contraction delay of motor units in rat's medial gastrocnemius muscle. *Biol. Sport* **5**, 285-295.
[113] Raikova, R., Krutki, P., Aladjov, H. & Celichowski, J. 2007 Variability of the twitch parameters of the rat medial gastrocnemius motor units—experimental and modeling study. *Comput. Biol. Med.* **37**, 1572-1581.
[114] Wilander, B. 1966 Active state durations of rat gastrocnemius muscle. *Acta Physiol. Scand.* **68**, 1-17.
[115] McPhedran, A.M., Wuerker, R.B. & Henneman, E. 1965 Properties of Motor Units in a Homogeneous Red Muscle (Soleus) of the Cat. *J. Neurophysiol.* **28**, 71-84.
[116] Wuerker, R.B., McPhedran, A.M. & Henneman, E. 1965 Properties of motor units in a heterogeneous pale muscle (m. gastrocnemius) of the cat. *J. Neurophysiol.* **28**, 85-99.
[117] Bakels, R. & Kernell, D. 1993 Matching between motoneurone and muscle unit properties in rat medial gastrocnemius. *J. Physiol.* **463**, 307-324.
[118] Krutki, P., Celichowski, J., Lochyński, D., Pogrzebna, M. & Mrówczyński, W. 2006 Interspecies differences of motor units properties in the medial gastrocnemius muscle of cat and rat. *Arch. Ital. Biol.* **144**, 11-23.
[119] Krutki, P., Ciechanowicz, I., Celichowski, J. & Cywińska-Wasilewska, G. 2008 Comparative analysis of motor unit action potentials of the medial gastrocnemius muscle in cats and rats. *J. Electromyogr. Kinesiol.* **18**, 732-740.
[120] Mrowczynski, W., Celichowski, J. & Krutki, P. 2006 Interspecies differences in the force-frequency relationship of the medial gastrocnemius motor units. *J. Physiol. Pharmacol.* **57**, 491-501.
[121] Burke, R.E. 1967 Motor unit types of cat triceps surae muscle. *J. Physiol.* **193**, 141-160.
[122] Burke, R.E. 1968 Firing patterns of gastrocnemius motor units in the decerebrate cat. *J. Physiol.* **196**, 631-654.
[123] Devanandan, M.S., Eccles, R.M. & Westerman, R.A. 1965 Single motor units of mammalian muscle. *J. Physiol.* **178**, 359-367.

[124] Emonet-Denand, F., Hunt, C.C., Petit, J. & Pollin, B. 1988 Proportion of fatigue-resistant motor units in hindlimb muscles of cat and their relation to axonal conduction velocity. *J. Physiol.* **400**, 135-158.
[125] Hammarberg, C. & Kellerth, J.O. 1975 Studies of some twitch and fatigue properties of different motor unit types in the ankle muscles of the adult cat. *Acta Physiol. Scand.* **95**, 231-242.
[126] Olson, C.B. & Swett, C.P., Jr. 1971 Effect of prior activity on properties of different types of motor units. *J. Neurophysiol.* **34**, 1-16.
[127] Winters, J.M. 1995 An Improved Muscle-Reflex Actuator for Use in Large-Scale Neuromusculoskeletal Models. *Ann. Biomed. Eng.* **23**, 359-374.
[128] Zajac, F.E. & Winters, J.M. 1990 Modeling Musculoskeletal Movement Systems: Joint and Body Segmental Dynamics, Musculoskeletal Actuation, and Neuromuscular Control. In *Multiple Muscle Systems: Biomechanics and Movement Organization* (eds. J.M. Winters & S.L.-Y. Woo). New York, NY, Springer.